Astron. Astrophys. 315, L317–L320 (1996)

ASTRONOMY
AND
ASTROPHYSICS

Very cold dust associated with molecular gas⋆,⋆⋆

R.J. Laureijs[1], L. Haikala[2], M. Burgdorf[1], F.O. Clark[3], T. Liljeström[2], K. Mattila[2], and T. Prusti[1]

[1] ISO Science Operations Centre, Astrophysics Division of ESA, Villafranca, Apdo 50727, E-28080 Madrid, Spain
[2] Observatory, P.O. Box 14, FIN-00014 University of Helsinki, Finland
[3] Geophysics Directorate - Phillips Laboratory, GPOB 29 Randolph Road, Hanscom Air Force Base, MA 01731, USA

Received 15 July 1996 / Accepted 3 September 1996

Abstract. We report the detection of very cold dust in a small and isolated dust cloud. Observations at 60, 90, 135, and 200 μm show a constant surface brightness ratio I_{135}/I_{200} and a flattening of I_{90}/I_{200} towards the cloud centre. The dust temperature derived from the far-infrared colours can be confined to the range of 12-15 K assuming a λ^{-2} dust emissivity. The 60 μm emission comes mainly from outer dust layers surrounding the core. We infer that a fraction of the power in the 90 μm band comes from the warmer grain component also causing I_{60}. This fraction is approximately equal to the total power in the 60 μm band.

The cloud is also detected in ^{12}CO, ^{13}CO, ^{18}CO, HCO$^+$ and CS. The detections indicate that the dust emission is associated with a molecular cloud core where $n(H_2) \geq 3\,10^4$ cm^{-3}. Using the column density derived from the molecular observations we find an extinction cross section per H-atom of 4.1–9.5 cm^2/H-atom.

Key words: interstellar medium: dust, extinction – interstellar medium: clouds – interstellar medium: molecules

1. Introduction

The far infrared signature of the large grains that give rise to the visual extinction and the bulk of the total dust mass has recently been refined by Boulanger et al. (1996) using data collected by the cosmic background explorer (COBE). These measurements are of importance for modelling the dust composition and for deriving the mass of dust clouds from far infrared observations (Hildebrand 1983). Unfortunately, due to the poor resolution of COBE this result stricktly applies to dust in the diffuse interstellar medium associated with HI. Dust in denser regions can only be detected on smaller angular scales of order a few arcminutes or less.

The first far-infrared data of dense clouds were collected by the KAO but due to the limited field of view and chop throw, the cloud's background level was hard to determine. In addition, the observations were biased by the presence of infrared emitting embedded young stellar objects (Keene et al. 1983).

IRAS provided a better spatial resolution than COBE but was still not able to determine directly the large grain temperature in dense clouds due to its limiting wavelength coverage in the far-infrared. The four IRAS bands at 12, 25, 60 and 100 μm were not sufficient to distinguish the large grain component from other dust components predominantly emitting in the IRAS 12, 25, and 60 μm bands. Only upper temperature limits could be derived in dense regions where the 60 μm emission was found to be absent (Laureijs, Clark & Prusti, 1990).

The photometer (ISOPHOT, Lemke et al. 1996) on board of the Infrared Space Observatory (ISO) offers 11 filters in the 40-240 μm wavelength range with a spatial resolution comparable to that of IRAS. The far-infrared wavelength coverage of ISOPHOT should be suitable to detect the far-infrared signature of cold dust at several wavelengths.

2. Target selection and observations

We have selected from the IRAS ISSA database a 100 μm emission peak for which the brightness ratio I_{60}/I_{100} in the centre is less than 0.05. The region with low I_{60}/I_{100} is less than 20' in extent, a suitable target for follow up with ISO.

Inspection of the ESO/SERC films shows that the target is situated in a region with patches of visual obscuration. On a larger scale the target is located within the triangle formed by the Chamaeleon I, II, and III clouds. We infer that the 100 μm emission peak is likely a small dense dust cloud only emitting beyond 60 μm. The cloud appears to be associated with the Chamaeleon complex of clouds situated at a distance of 140 pc (Franco, 1991).

Send offprint requests to: R.J. Laureijs

⋆ Based on observations made with ISO, an ESA project with instruments funded by ESA Member States (especially the PI countries: France, Germany, the Netherlands and the United Kingdom) and with the participation of ISAS and NASA

⋆⋆ Based on observations with SEST

Table 1. Summary of ISOPHOT observations

Filter	λ_c μm	Raster	stepsize inxcross	Camera
C_60	63	15x3	138"x92"	C100
C_90	89	15x3	138"x92"	C100
C_135	155	11x3	180"x92"	C200
C_200	210	11x3	180"x92"	C200

Table 2. Comparison COBE versus ISOPHOT background observations

Filter	ISOPHOT MJy/sr	COBE MJy/sr	Ratio
C_60	5.2	7.4	0.7
C_90	10	10	1.0
C_135	67.0	31	2.2
C_200	65.5	28	2.3

2.1. Infrared observations

With the ISOPHOT C100 and C200 cameras commanded using observation template number 22 (P22, Klaas et al. 1994) we have obtained scans across the cloud in staring raster mode. The filter and raster specifications have been tabulated in Table 1.

The rasters were centred on the cloud's centre position (RA(1950) = $12^h\,13^m\,26^s$, Dec(1950) = $-79°00'\,29$") with a position angle of 90° so that the in-scan points were obtained at a constant declination. As a consequence of this scanning mode, the camera arrays (which are fixed with respect to the spacecraft orientation) were tilted with a position angle of 171°. We have neglected this tilt in our analysis and assumed that the arrays were aligned with the raster frame. Detailed camera and filter specifications can be found in Laureijs, Richards & Krüger (1996).

The cross-scan raster steps were smaller than the dimension of the camera arrays which ensures detector overlap of the cross scans. This redundancy has been used to correct for inconsistencies in flat fielding due to detector responsivity drifts.

2.2. Molecular observations

The molecular observations were made with the 15 m Swedish-ESO Submillimeter Telescope (SEST) in La Silla, Chile, in the night of June 13, 1996. A SSB 3 mm and 2 mm SIS receiver was used. These had receiver temperatures ranging from 100K to 140K at the observed frequencies, respectively. The velocity resolution of the spectrometer was approximately 0.2 km s^{-1} at 3 mm and 0.15 at 2 mm. The system temperature reduced to outside of the amosphere ranged from 150K (HCO^+ J=1→0) to 400 K (^{12}CO, J=1→0). The half-power beamwidth of the telescope is 50" at 3 mm.

The observations were made in frequency switching mode (8 MHz at 3 mm and 16 MHz at 2mm). The following molecules and transitions were observed: ^{12}CO, J=1→0 (16 positions), ^{13}CO, J=1→0 (a map of 53 positions) and C^{18}O, J=1→0 (a map of 70 positions). One position was observed in CS J=2→1 and CS J=3→2, HCO^+ J=1→0 and DCO^+ J=2→1 . The maps consist of rectangular grids in RA and Dec using 1′ gridspacings.

3. Infrared Data Processing and Calibration

The signals (in V/s) per pixel have been obtained from the raw data by fitting a first order polynomial to the integration ramps after correcting for electronics non-linearities and cosmic ray hits. The weighted mean signal per raster point has been computed after removing signal outliers and subtracting the detector dark signal. The arrays have been flatfielded by comparing the raster scans of the individual detector pixels. The signal gain of each pixel has been adjusted such that a best match is obtained with respect to a reference pixel. For both arrays pixel 1 has been used as reference.

To obtain one-dimensional slices of the cloud we have averaged at each given position along the central scan all the detector signals that fall inside a square box of 180″ (4 C100 pixel widths) for the C_60 and C_90 filters. A similar method was used for the C_135 and C_200 filters but here we used a box of 2 C200 pixel widths. This gives an effective resolution of about 4′ along the scan direction at all measured wavelengths.

As part of the standard observation procedure, each raster scan in a given filter band is bracketed by two identical measurements of the fine calibration source (FCS) which is a grey body inside the ISOPHOT instrument. The signals were converted to surface brightness values (in MJy/sr) by taking the mean value of the two FCS calibration factors. By the time of writing this letter the FCS calibrations against astronomical standards have not been finalized. Therefore the uncertainties in the C200 filters can be as high as 100%.

To assess the photometric uncertainties in this preliminary stage of the ISOPHOT calibration we compared the background levels in our scans with COBE observations taken at the same position with the same solar elongation of 96° (Table 2). DIRBE brightness values were obtained by averaging over a circular area of 1.5° degrees diameter centred on the cloud. From the IRAS maps and by integrating over different circular areas with COBE we ensured that there are no strong emission sources in the area except for the cloud complex itself. The DIRBE background values have been interpolated to obtain the emission in the ISOPHOT bands by fitting a modified blackbody $\nu^2 B_\nu(T = 17.5K)$ through the 100, 140 and 240 μm DIRBE bands.

The ISOPHOT C_60 and C_100 bands are in reasonable agreement with DIRBE, but the C_135 and C_200 bands show a discrepancy up to a factor of 2.3. The lower DIRBE values can

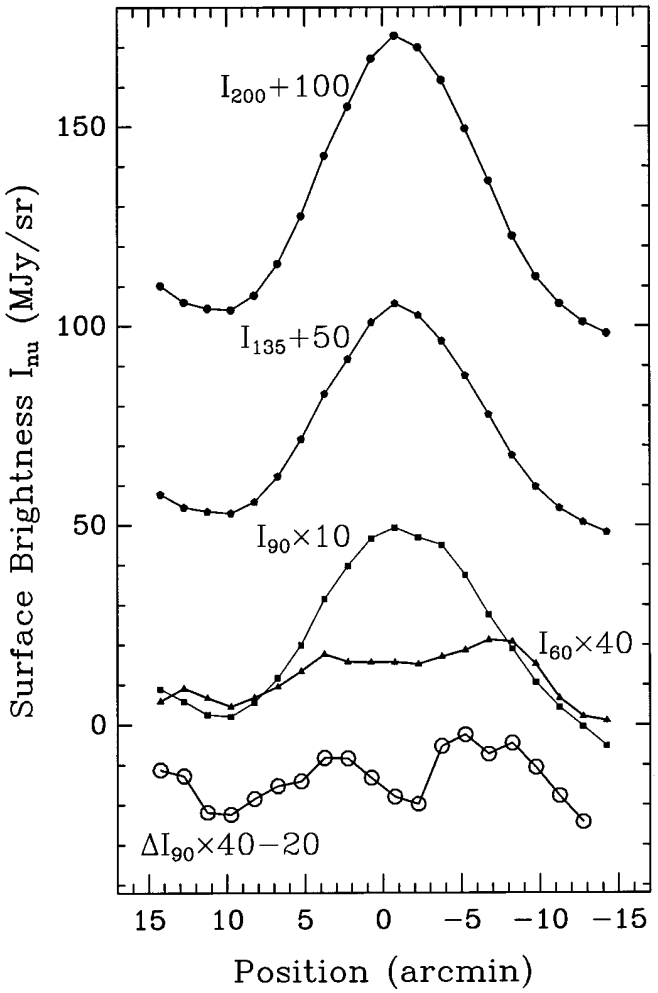

Fig. 1. Far-infrared scans of the cloud obtained at constant declination, Eastern direction is to the left. ΔI_{90} is the residual 90 μm emission after subraction of the scaled I_{200} profile

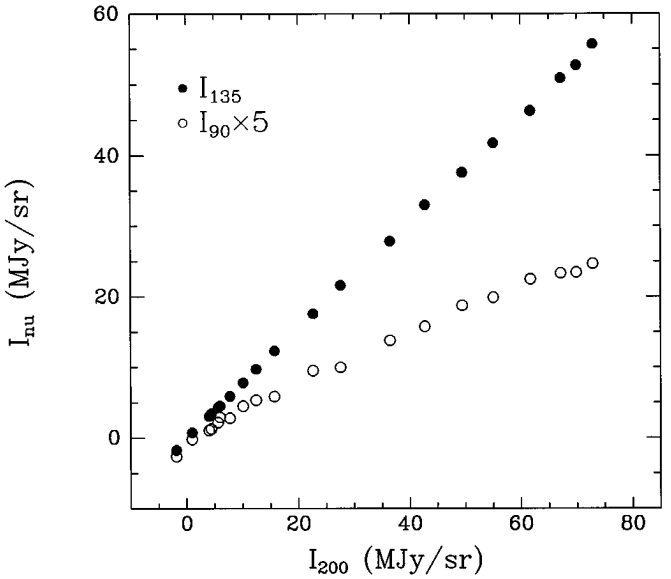

Fig. 2. The variation of I_{90} and I_{135} as a function of the surface brightness in C_200, I_{200}

be expected due to the unknown cloud structure immediately outside the main emission peak with spatial sizes smaller than the DIRBE resolution. Nevertheless we conservatively adopt a factor 2.3 lower C_135 and C_200 brightness values as part of the photometric uncertainty in these two filters. We add an independent 20% relative uncertainty between the bands.

4. Results and discussion

Far-infrared profiles of the cloud after background subtraction are presented in Fig. 1. The detection of a regular cloud core is evident from the emission in the C_135 and C_200 bands. The two profiles appear very similar with a full width at half maximum of 10′. Most striking is the absence of a 60 μm emission peak in the centre of the cloud as already indicated by the IRAS data. The profile suggests that the 60 μm emission comes mainly from the outer cloud layers surrounding the core. At 90 μm the surface brightness in the centre is more prominent. The peak is at position 0 as expected from the IRAS 100 μm data.

To investigate the far-infrared colours of the cloud we have plotted in Fig. 2 I_{135} and I_{90} as a function of I_{200}. The tight linear correlation between I_{135} and I_{200} demonstrates that there are no significant temperature variations in the dust causing I_{135} and I_{200}.

We observe a flattening in I_{90}/I_{200} which suggests a temperature drop towards the cloud centre. In view of the constant I_{135}/I_{200} this can only be due to a warmer component in the outer parts of the cloud. Assuming that all I_{90} in the centre of the cloud comes from the same emission component as the one causing I_{135} and I_{200}, we computed the excess 90 μm emission ΔI_{90} according to:

$$\Delta I_{90} = I_{90} - I_{200} * 0.067 \quad \text{MJy/sr}, \tag{1}$$

where the factor 0.067 is I_{90}/I_{200} measured in the cloud centre. The ΔI_{90} profile has been included in Fig. 1. The profile is remarkably similar to that of I_{60}. In addition, we find an average ratio of 1.1 ± 0.3 between the in-band powers (=$\Delta\lambda I_\lambda$) of ΔI_{90} and the 60 μm band [1]. Given the fact that the equivalent width of C_90 is substantial ($\Delta\lambda$ = 56 μm), we conclude that ΔI_{90} is probably due to the dust component which also emits at 60 μm.

In Table 3 we summarize the temperatures derived from the far-infrared brightness ratios. The I_{90}/I_{200} colour temperature has been measured both in the centre and near the edge of the cloud. The values for I_{135}/I_{200} and I_{90}/I_{200} in the cloud centre yield more consistent temperatures for a λ^{-2} emissivity law. Including all uncertainties, we conclude that the most likely dust temperature in the cloud is in the range 11.9-15.3 K with a λ^{-2} emissivity law.

[1] This result is independent of the uncertainty in the absolute calibration of C_200 because incorrect calibration would only affect the scaling factor leaving ΔI_{90} unchanged.

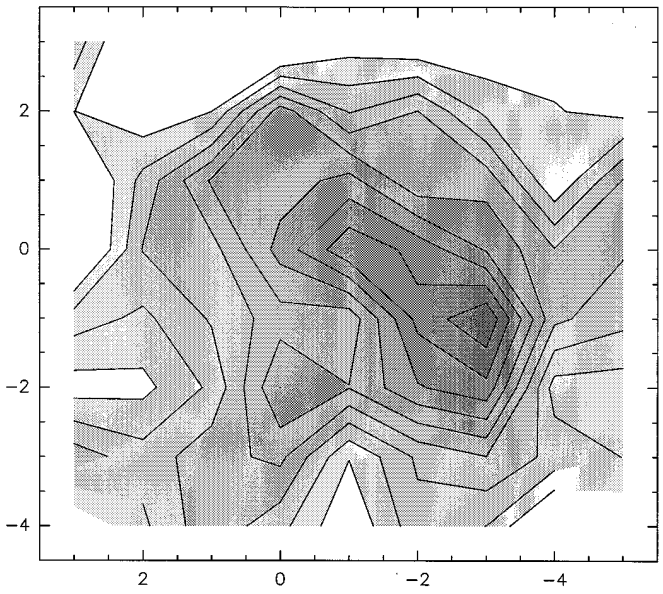

Fig. 3. $C^{18}O$ (J = 1 – 0) integrated T_R^* map. The offsets are given in arcminutes with respect to position (RA(1950) = $12^h\ 13^m\ 26^s$, Dec(1950) = $-79°00'\ 29"$); highest contour: 1.1 K kms^{-1}, step: 0.12 K kms^{-1}

Table 3. Measured dust temperatures assuming two different far-infrared dust emissivity power laws, "regression" means derived by linear regression analysis

Colour	Brightness Ratio	$T(\lambda^{-1})$ K	$T(\lambda^{-2})$ K	comment
I_{135}/I_{200}	$0.76^{+0.15}_{-0.15}$	$16.2^{+2.7}_{-2.3}$	$13.5^{+1.8}_{-1.7}$	regression
I_{90}/I_{200}	$0.067^{+0.087}_{-0.013}$	$14.0^{+2.4}_{-0.5}$	$12.4^{+1.8}_{-0.5}$	centre
I_{90}/I_{200}	$0.12^{+0.16}_{-0.024}$	$15.6^{+3.1}_{-0.7}$	$13.6^{+2.3}_{-0.5}$	edge

The SEST ^{13}CO observations show strong lines ($T_R^* dV$ = 4 Kkm/s) but little structure in the $8' \times 7'$ area surveyed around the centre position. All ^{12}CO lines are self-absorbed in that area. A small size (6′ by 4′) core centred on position ($-2'$, $-1'$) has been detected in $C^{18}O$ (Fig. 3). The offset is consistent with the peak brightness offset observed in the C_135 and C_200 bands.

A column density has been determined from the $C^{18}O$ observations assuming optically thin $C^{18}O$ lines. Using the conversion between $C^{18}O$ column density and H_2 as given by Harjunpää & Mattila (1996) for the Coalsack, we find a peak column density of $N(H_2)$=1.4 10^{22} cm^{-2}. At a distance of 140 pc the derived mass of the core is 9 $M_\odot$.

Observations on the $C^{18}O$ peak position ($-2'$,$-1'$) in CS J=2→1 and CS (J=3→2), HCO^+ J=1→0 and DCO^+ J=2→1 have shown that the core can be detected in all but the DCO^+ J=2→1 transition. As the core was detected in both the observed CS transitions and in $HCO^+$the density in the core must be in excess of $n(H_2)$ = 3 10^4 cm^{-3} which is the estimated effective critical density of the CS J=2→1 transition.

Combining the column density and temperature determination we derive the extinction cross section per H nucleus which relates the far-infrared opacity τ_λ with the hydrogen column density (Hildebrand, 1983). Depending on the assumed emissivity we find for λ = 200 μm:

$$\frac{\tau_\lambda(T_d = 16.2\,\mathrm{K})}{N_H} = (1.7 - 4.0)\,10^{-26}\ \mathrm{cm^2/H\text{-}atom} \qquad (2)$$

for a λ^{-1} emissivity, or

$$\frac{\tau_\lambda(T_d = 13.5\,\mathrm{K})}{N_H} = (4.2 - 9.5)\,10^{-26}\ \mathrm{cm^2/H\text{-}atom} \qquad (3)$$

assuming a λ^{-2} emissivity. We fixed the temperature in the calculation and considered the calibration uncertainty in I_{200} to determine the range.

Draine & Lee (1984) derive τ_λ/N_H = 6.6 10^{-26} cm^2/H-atom for astronomical silicate and 9.5 10^{-26} cm^2/H-atom for graphite grains, assuming a Mathis et al. (1978) dust composition. Our observed values of τ_λ/N_H are on the lower side but still in agreement with predictions from this standard "classical dust" model.

Acknowledgements. The ISOPHOT instrument was funded by the Deutsche Argentur für Raumfahrtangelegenheiten and the Max Planck Gesellschaft. The ISOPHOT data were reduced using PIA, a joint development by the ESA Astrophysics Division and the ISOPHOT consortium led by the Max Planck Institute for Astronomy, Heidelberg. We thank W. Reach for providing the COBE background data and E. Dwek for stimulating discussions. We thank R. Verschoor for crucial contributions to the ISO data processing.

References

Boulanger F., Abergel A., Bernard J.-P., Burton W.B., Désert F.-X, Hartmann D., Lagache G., Puget J.-L 1996 A&A *in press*
Draine B.T., Lee H.M. 1984, ApJ 285, 89
Franco G.A.P. 1991, A&A 251, 581
Harjunpää P., Mattila K. 1996, A&A 305, 920
Hildebrand R.H. 1983, QJRAS 24, 267
Keene J., Davidson J.A., Harper D.A., Hildebrand R.H., Jaffe D.T., Loewenstein R.F., Low F.J., Pernic R. 1983, ApJ 274, L34
Klaas U., Krüger H., Heinrichsen I., Heske A., Laureijs R.J., 1994, ISOPHOT Observer's Manual, version 3.1.
Laureijs R.J., Clark F.O., Prusti T. 1991, ApJ 372, 185
Laureijs, R.J., Richards, P.J., Krüger H. 1996, ISOPHOT Data Users Manual, version 2.0, SAI/95-220/Doc
Lemke D. et al. 1996, A&A, *this issue*
Mathis J.S., Rumpl W, Nordsieck K.H. 1977, ApJ 217, 425